https://doi.org/10.46813/2026-165-068

APPROXIMATION-BASED ALGORITHM FOR NEUTRON-GAMMA DISCRIMINATION

V.O. Novgorodtsev, O.V. Kolesnikov
Institute for Scintillation Materials, National Academy of Sciences of Ukraine, Kharkiv, Ukraine
E-mail: novgorodvl@isma.kharkiv.ua

A novel Exponential Function Approximation (EFA) algorithm for neutron-gamma discrimination in organic scintillation detectors is proposed. The algorithm is based on approximating the tail of the scintillation pulse using a basis function represented by the sum of two exponential components with fixed time constants. The algorithm parameters were optimized by maximizing the figure of merit (FOM) for neutron-gamma discrimination. Experimental validation using scintillation pulses from a PuBe source demonstrated that the proposed algorithm increases the FOM from 1.16 to 1.43 (by 23%) in the energy range of 50…100 keVee and from 1.39 to 2.00 (by 44%) in the energy range of 100…200 keVee compared with the conventional charge integration (CI) method. The discrimination performance achieved by the EFA algorithm in the 50…100 keVee range is comparable to that provided by the CI method in the 100…200 keVee range, indicating a reduction in the minimum energy threshold for neutron-gamma discrimination and corresponding to an approximately 12% increase in the number of reliably identified neutron events. The proposed algorithm generalizes the conventional CI method and reduces to it in the limiting case where the basis function is identically equal to unity. An implementation of the EFA algorithm with computational complexity approaching that of the CI method is proposed.

PACS: 29.40.Mc; 78.70.Ps; 78.55.Kz; 78.47.jd; 02.60.Gf

INTRODUCTION

Organic single crystals are widely used for neutron–gamma discrimination in mixed radiation fields due to the different interaction mechanisms of neutrons and gamma rays with the scintillation material [1–4]. Fast neutrons interact predominantly through elastic scattering on hydrogen nuclei, producing recoil protons that create regions of high ionization density and scintillation pulses with a significant contribution from the slow component [1, 4–6]. In contrast, gamma rays in the energy range relevant to neutron–gamma discrimination interact mainly through the Compton effect, producing recoil electrons that generate regions of lower ionization density and pulses with a smaller slow-component contribution [1, 2, 4]. These differences in the temporal structure of scintillation pulses form the basis of pulse shape discrimination (PSD) methods [1, 4, 7, 8].

In practice, PSD is implemented by calculating a scalar parameter that is sensitive to the contribution of the slow scintillation component. The most widely used approach is the Charge Integration (CI) method, in which the PSD parameter is defined as the ratio of the integral of the pulse tail to the integral of the entire pulse [8–10].

In the general case, the CI method is defined by four integration time boundaries. However, it is most commonly implemented using three independent parameters by setting the end of the tail integration window equal to the end of the total integration window [8, 9, 11–15]. Implementations with two non-overlapping integration windows have also been reported [16, 17].

The quality of neutron-gamma discrimination is evaluated using scatter plots of the PSD parameter and histograms of its distribution for selected energy intervals [1, 8, 9]. The primary quantitative criterion is the Figure of Merit (FOM), defined as the ratio of the distance between the neutron and gamma peak centroids to the sum of their full widths at half maximum (FWHM) [9, 18–20].

The main limitation of the CI method is the significant degradation of discrimination performance in the low-energy region of the spectrum due to a reduced signal-to-noise ratio and weaker differences between neutron and gamma pulse shapes [1, 8, 9, 12]. To improve PSD performance, energy-dependent discrimination methods, adaptive selection of integration windows, and machine-learning algorithms have been proposed [9, 12, 21–23]. Nevertheless, reliable neutron–gamma discrimination at energies below 100 keVee remains a challenging task.

The aim of this work is to improve neutron–gamma discrimination by developing a PSD algorithm based on Exponential Function Approximation (EFA) of the tail portion of the scintillation pulse. The performance of the proposed algorithm was experimentally evaluated using a detector based on a trans-stilbene single crystal and compared with the conventional CI method.

1. MATERIALS AND METHODS

Experimental studies were performed using a scintillation detector based on a cylindrical trans-stilbene single crystal with a diameter of 25 mm and a height of 25 mm, fabricated from a 65 mm diameter crystal grown by the Bridgman method. To improve light collection, the crystal was wrapped with two layers of PTFE reflector film, and optical coupling to the photodetector was provided using Sylgard 186 silicone compound.

Scintillation events were detected with a Hamamatsu R6231 photomultiplier tube (PMT) operated at a bias voltage of 780 V. The PMT anode signal was amplified

by a broadband amplifier and digitized using a 12-bit CAEN DT5720 analog-to-digital converter with a sampling rate of 250 MS/s. The dynamic response of the detection chain was primarily determined by the Hamamatsu R6231 PMT, which has a pulse rise time of approximately 8.5 ns [24].

The recorded and digitized scintillation pulses were stored as event files for subsequent offline processing and analysis. Pulses exhibiting saturation or pile-up were rejected. Energy calibration of the detector was performed using a ^{137}Cs source spectrum, based on the position of the Compton edge corresponding to 477 keVee.

Mixed neutron-gamma radiation was obtained from a Pu–Be source without additional shielding in the presence of natural gamma background. Mixed neutron–gamma radiation was obtained from a Pu–Be source without additional shielding in the presence of natural gamma background. The event energy was determined from the total charge of the scintillation pulse integrated over the 0…700 ns time window relative to the pulse onset. The pulse start time (t_0) was defined by the threshold-crossing point of the signal, corresponding to an energy of approximately 30 keVee. The average counting rate was 40…60 pulses/s for the Pu–Be source and 200…300 pulses/s for the ^{137}Cs source.

Processing of event files, pulse approximation, calculation of PSD parameters, statistical analysis, and graph plotting were performed using custom-developed software implemented in the Python programming language [25].

2. RESULTS AND DISCUSSION

Most pulse shape discrimination methods exhibit a degradation in neutron-gamma discrimination performance as the energy of the detected events decreases. In this work, it is hypothesized that one of the reasons for this is the presence of a stochastic component in the scintillation signal, which manifests itself as rapid random amplitude fluctuations that are most pronounced in the tail of the pulse. These stochastic fluctuations are associated with statistical variations in the number of generated and detected scintillation photons, photon transport and light collection processes, photoelectron conversion in the photodetector, and electronic noise in the readout chain [1, 5, 9, 26, 27]. Despite the different physical origins of these processes, their total contribution can be considered, to a first approximation, as an additive random component of the signal.

2.1. DETERMINATION OF THE TIME PARAMETERS OF SCINTILLATION PULSES

Fig. 1 shows the recorded scintillation pulses produced by neutrons (1) and gamma rays (2) corresponding to an energy of 50 keVee.

The time parameters of organic scintillators are commonly determined using the single-photon technique, which allows the characteristics of the intrinsic scintillation pulse to be measured without distortion by the electronic readout chain [28–32].

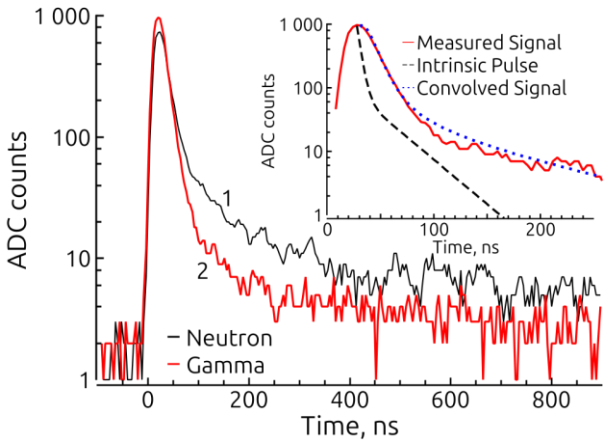


Fig. 1. Recorded scintillation pulses produced by neutrons (1) and gamma (2) at 50 keVee. Inset: intrinsic scintillation pulse (dashed line), its convolution with the impulse response of the electronic readout chain (dotted line), and the measured signal (solid line)

In real detector systems, the shape of the recorded signal, *Y(t)*, is the convolution of the intrinsic scintillation pulse, *I(t)*, determined by the scintillation material, with the impulse response of the electronic readout chain, *h(t)*:

$$Y(t) = \int_0^T I(t)\,h(t-\tau)\,\mathrm{d}\tau, \qquad (1)$$

where *T* is the pulse duration, *Y(t)* is the signal at the ADC input, *I(t)* is the intrinsic scintillation pulse, *h(t)* is the impulse response of the electronic readout chain.

As a simplified approximation, the intrinsic scintillation pulse and the impulse response of the electronic readout chain are assumed to be described by exponential functions. In this case, their convolution is given by:

$$Y(t) = \frac{I_0\tau_s}{\tau_s-\tau_e}\left(\exp\left(-t/\tau_s\right)-\exp\left(-t/\tau_e\right)\right), \qquad (2)$$

where τ_p is the time constant of the intrinsic scintillation pulse, and τ_e is the effective time constant of the electronic readout chain.

As an example, the inset of Fig. 1 shows the measured signal at the ADC input and the calculated pulse obtained by convolving the intrinsic scintillation pulse with the impulse response of the electronic chain with a time constant of 9 ns.

Since scintillation pulses of organic single crystals are typically described by two or three exponential components [18, 28, 33–35] or by non-exponential functions [36–39], explicitly accounting for the convolution in Eq. (2) substantially complicates the model. Therefore, in this work the recorded scintillation pulse was described by the following model:

$$Y_r(t_i) = \mathrm{A}_{\mathrm{r},0} + \sum_{\mathrm{k}=1}^{3} A_{\mathrm{r,k}}\exp\left(-t_i/\tau_{\mathrm{r,k}}\right) + \mathrm{n}(t_i), \qquad (3)$$

$$Y_r(t_i) = \left(Y_r(t_1),\ldots,\mathrm{Y}_r(t_N)\right), \qquad (4)$$

where $r \in \{n,\gamma\}$ denotes the radiation type (*n* for neutrons and γ for gamma rays), $Y(t_i)$ is the pulse amplitude at discrete time $t_1,\ldots,\mathrm{t}_N$, A_0 is the constant baseline component, $A_k>0$ and $\tau_k>0$ are the amplitudes and time

constants of the exponential components *(k∈{1,2,3})*, respectively, and $n(t_i)$ is the stochastic component of the signal.

The resulting effective time constants characterize the temporal structure of the recorded signal, which is determined by the combined effects of scintillation kinetics and the time response of the measurement chain. Therefore, they can be used for quantitative comparison of scintillation pulse shapes. Accordingly, the recorded scintillation pulse is represented as the sum of a constant baseline and three exponential components:

$$Y_r\left(t_i\right)=\mathrm{A}_{\mathrm{r},0}+\sum_{\mathrm{k}=1}^{3}A_{\mathrm{r,k}}\exp\left(-t_i/\tau_{\mathrm{r,k}}\right). \qquad (5)$$

Direct approximation of each pulse using the model in Eq. (5) proved ineffective for accurate PSD (Fig. 2). Each recorded scintillation pulse was independently fitted in the selected tail interval using the sum of two exponential functions, with both amplitudes and time constants estimated by nonlinear least-squares fitting. For the 100…200 keVee range, an FOM of 0.74 was obtained, which is substantially lower than the value of 1.39 achieved by the classical CI method on the same dataset.

The scatter plots demonstrate the dependence of the fitting parameters on the radiation type; however, compact and well-separated clusters are not formed. The main reasons are the influence of the stochastic signal component and the poor conditioning of the nonlinear approximation problem: in a sum of exponentials, a change in the parameters of one component can be compensated by a change in another, which leads to an unstable determination of the parameters A_k and τ_k. This effect is particularly pronounced for low-energy events, where the relative contribution of statistical fluctuations increases due to the smaller number of photoelectrons [18, 20].

Moreover, direct fitting of each pulse requires the iterative solution of a nonlinear least-squares problem, making this approach computationally inefficient for real-time systems operating at moderate and high counting rates.

The objective of the subsequent processing stage is to construct a decision rule for neutron–gamma discrimination. To achieve this, common model parameters for both radiation types must be determined. A two-stage parameter estimation procedure was therefore employed.

In the first stage, averaged neutron and gamma pulses were constructed separately using at least 50 pre-classified events of each type. Assuming statistical independence of the events, averaging reduces the variance of the stochastic signal component in proportion to the number of pulses.

At the second stage, the averaged neutron and gamma pulses were approximated simultaneously within a single global least-squares problem, assuming identical time constants τ_k for both types of radiation, while the amplitudes A_k depend on the type of the registered event. This assumption is based on the fact that the differences between neutron and gamma pulses are determined primarily by the relative contributions of the exponential components, while their time constants vary only slightly [4, 13, 28].

Under these assumptions, the fitting functions for the averaged neutron and gamma pulses are given by:

$$y_r\left(t_i,\theta\right)=\mathrm{A}_0+\sum_{\mathrm{k}=1}^{3}A_{\mathrm{r,k}}\exp\left(-t_i/\tau_k\right), \qquad (6)$$

where $\theta=\left(A_0,\mathrm{A}_{\gamma 1},\mathrm{A}_{\gamma 2},\mathrm{A}_{\gamma 3},\mathrm{A}_{\mathrm{n}1},\mathrm{A}_{\mathrm{n}2},\mathrm{A}_{\mathrm{n}3},\tau_1,\tau_2,\tau_3\right)$ is the vector of model parameters.

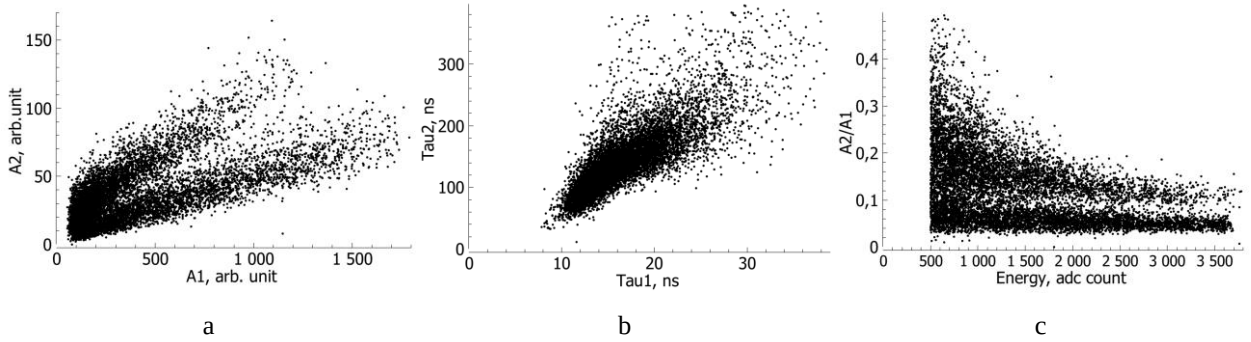
The model parameters were determined by minimizing the least-squares objective function:

$$J\left(\theta\right)=\sum_{i}^{N}\left(y_\gamma\left(t_i\right)-\hat{y}_\gamma\left(t_i,\theta\right)\right)^2+\sum_{i}^{N}\left(y_n\left(t_i\right)-\hat{y}_n\left(t_i,\theta\right)\right)^2, \qquad (7)$$

where $\hat{y}_\gamma$ and $\hat{y}_n$ are the averaged gamma-ray and neutron pulses, respectively.

Table 1 presents the results of the simultaneous fitting performed according to Eqs. (6), (7).

The results presented in Table 1 show that the estimated time constants τ_1, τ_2, and τ_3 remain nearly unchanged over the investigated energy range. The obtained values are consistent with previously reported data [13, 28, 30, 35], although the estimated fast-component time constant τ_1 is slightly larger. This is explained by the fact that the fitting was performed using recorded pulses, whose shape is affected by the dynamic response of the electronic readout chain.



a b c

Fig. 2. Results of the independent fitting of the tail portion of each scintillation pulse: a – estimated amplitude A2 as a function of A1; b – estimated time constant τ2 as a function of τ1; c – ratio A2/A1 as a function of pulse energy

Table 1

Parameters obtained from the simultaneous fitting of neutron and gamma scintillation pulses recorded with the trans-stilbene single-crystal detector over the 68…616 ns time interval

Energy, keVee	$A_{\gamma 1}$	$A_{\gamma 2}$	$A_{\gamma 3}$	$A_{\gamma 2}/A_{\gamma 3}$	A_{n1}	A_{n2}	A_{n3}	A_{n2}/A_{n3}	τ_1, ns	τ_2, ns	τ_3, ns
50	1	1.1	0.12	9.2	1.13	0.86	0.27	3.2	9.84	55.6	311
100	3.2	2.4	0.8	3.0	2.5	5.1	4.4	1.2	10.6	33.2	157
200	9.1	4.5	1.7	2.6	7.3	12.5	8.6	1.5	10.8	32.9	158
300	15.1	7.2	2.2	3.3	10.6	22.9	8.7	2.6	10.2	37.8	195
400	23.4	7.1	2.4	3.0	21.6	21.8	14.1	1.5	11.5	39.1	175
500	30.1	9.1	4.2	2.2	26.1	28.9	18.2	1.6	11.1	35.7	151
600	35.5	11.1	4.7	2.4	31.3	34.4	21.3	1.6	11.2	35.0	156.4
800	52.5	16.1	4.2	3.8	56.2	43.81	21.58	2.0	11.7	46.9	201.07
Average	–	–	–	3.3	–	–	–	1.9	10.9	39.5	188.1

Therefore, the obtained time constants should be regarded as effective parameters of the recorded signal rather than intrinsic scintillation time constants.

The influence of the radiation type is primarily reflected in the amplitudes of the individual exponential components. Therefore, in developing the EFA algorithm, we assume that the main differences between neutron and gamma events are determined by the ratio of the amplitudes of the slow components, A_2 and A_3, which form the tail of the scintillation pulse, relative to the amplitude of the fast component A_1. Accordingly, the slow component of the scintillation pulse, which forms the pulse tail and is associated with delayed luminescence, is represented as the sum of two exponential functions:

$$\hat{y}_i \approx A_x s_i, \tag{8}$$

$$s_i = \left(k \cdot \exp\left(-t_i / \tau_2\right) + \exp\left(-t_i / \tau_3\right)\right), \tag{9}$$

where $\hat{y}_i$ is the approximation of the scintillation pulse, s_i is the basis function, τ_2, τ_3 are effective time constants reflecting the combined influence of the scintillation material and the electronic readout chain, k is the ratio of the slow-component intensities, and A_x is the scaling coefficient representing the contribution of the slow component, which depends on the type of the recorded radiation.

After calibration, τ_2 and τ_3 remain fixed, and only the linear parameter A_x is estimated for each newly recorded pulse. Since the model is linear with respect to A_x, this parameter is determined by the least-squares method without nonlinear fitting:

$$A_x = \frac{\sum_i y_i s_i}{\sum_i s_i^2}, \tag{10}$$

where y_i is the recorded pulse.

When the values of the basis function s_i have been precomputed according to Eq. (9), calculating A_x using Eq. (10) differs from calculating the integrals in the conventional CI method only by one additional multiplication for each sampled point. Consequently, the EFA algorithm has the same order of computational complexity as the CI method. This makes the EFA algorithm suitable for implementation on the same hardware and software platforms used for CI, including FPGA-based systems, and for real-time scintillation signal processing.

Since the information about the radiation type is determined by the relative contribution of the slow scintillation components with respect to the fast component, the neutron–gamma discrimination parameter is defined as the ratio of the estimated coefficient A_x to the amplitude of the fast component A_1:

$$\mathrm{PSD} = \frac{A_x}{A_1}. \tag{11}$$

Thus, the proposed EFA algorithm calculates the PSD parameter for each recorded pulse using Eqs. (10) and (11). Conceptually, the EFA algorithm is closely related to the conventional CI method, since in both approaches the PSD parameter is determined by the relative contribution of the pulse tail, which contains the slow scintillation components sensitive to the radiation type, with respect to the fast initial part of the pulse, which depends much less on the radiation type.

However, unlike the CI method, the proposed approach estimates the contribution of the pulse tail by projecting the signal onto the basis function defined by Eqs. (8) and (9). From a mathematical perspective, the CI method can therefore be regarded as the simplest special case of the proposed EFA approach, corresponding to a constant basis function, $s_i \equiv 1$, in Eq. (8).

One reason for the improved neutron–gamma discrimination achieved by the EFA method is the use of a weighting function that accounts for the temporal structure of the pulse tail. In the conventional CI method, integration over the tail window is performed with equal weights assigned to all sampled points:

$$Q_{\mathrm{slow}} = \sum y_i. \tag{12}$$

The recorded scintillation pulse can be represented as the sum of a useful signal and a stochastic component. In the tail region of the pulse, where $t \gg \tau_1$, the amplitude of the scintillation signal decreases significantly, whereas the variance of the noise component remains nearly constant (see Fig. 1). As a result, samples acquired at later times contain progressively less information about the radiation type while still contributing to the numerical value of the PSD parameter.

Therefore, increasing the integration window accumulates both the useful signal and the stochastic component. A longer integration interval increases the difference between the neutron and gamma pulse integrals, thereby increasing the separation between the neutron and gamma peaks in the PSD histogram and improving the FOM. At the same time, it increases the contribution of the stochastic component, resulting in a larger spread of the PSD parameter and broader peaks, which reduces the FOM. A similar dependence of the FOM on the integration window width was also observed experimentally in [40], supporting the proposed interpretation.

2.2. OPTIMIZATION OF THE PROPOSED ALGORITHM PARAMETERS

The EFA algorithm contains five parameters determined during the optimization stage: the start (t_{start}) and end (t_{end}) of the fitting interval, the ratio of the slow-component intensities ($k = A_2/A_3$), and the time constants τ_2 and τ_3. The optimization criterion was the neutron-gamma discrimination quality parameter FOM, while the parameter ranges were selected based on the results of the simultaneous fitting presented in Table 1.

The optimization was performed in stages. First, the optimal fitting time interval was determined. If t_{start} was too small, the fitting interval included the fast pulse component; if it was too large, part of the information contained in the slow components was lost. The upper boundary, t_{end}, was chosen as a compromise between preserving the informative part of the pulse tail and limiting the accumulation of the stochastic signal component.

For each pair of t_{start} and t_{end}, the parameters k, τ_2, and τ_3 were optimized sequentially while keeping the other two parameters fixed and selecting the value that maximized the FOM. This procedure was repeated iteratively until the FOM stabilized. In practice, convergence was achieved after two iterations, indicating that the maximum within the search region had been reached.

Since the 50…100 keVee energy interval is the most critical for evaluating the performance of the EFA algorithm, the optimization results presented below correspond to this energy range. The dependence of the FOM on the fitting time interval (t_{start} = 44…76 ns, t_{end} = 200…600 ns) is presented in Table 2, while the dependence on the parameters k, τ_2, and τ_3 is shown in Fig. 2.

Table 2

Dependence of the FOM on the boundaries of the scintillation pulse fitting interval in the EFA algorithm

t_{start}, ns	t_{end}, ns				
	200	300	400	500	600
44	1.63	1.68	1.69	1.70	1.70
52	1.76	1.81	1.82	1.83	1.83
60	1.90	1.94	1.95	1.95	1.95
68	1.89	1.92	1.91	1.90	1.90
76	1.81	1.82	1.81	1.80	1.79

The analysis of Table 2 shows that the FOM strongly depends on the selected fitting time interval. The maximum value is achieved at t_{start} = 60 ns: smaller values include the fast pulse component, whereas larger values result in the loss of the informative part of the slow component. The influence of the upper boundary, t_{end}, is less pronounced, as the FOM remains nearly unchanged for t_{end}>400 ns. Therefore, the interval t_{start} = 60 ns and t_{end} = 400 ns was selected as the optimal fitting interval.

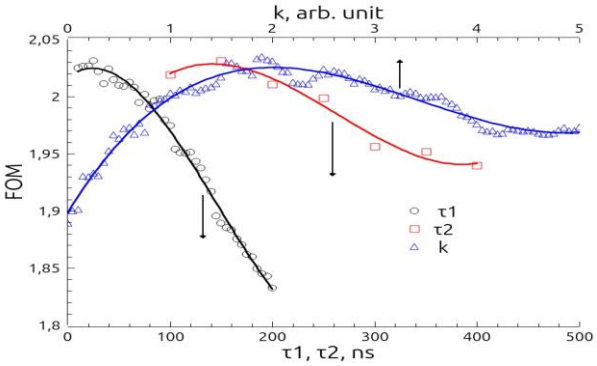


Fig. 3. Effect of the EFA algorithm parameters k, τ_2, and τ_3 on the FOM

The FOM dependencies on k, τ_2, and τ_3, shown in Fig. 3, exhibit well-defined maxima, confirming the existence of an optimal set of EFA algorithm parameters. The obtained optimal values are in good agreement with the results of fitting the averaged scintillation pulses (see Table 1), confirming the validity of the adopted scintillation pulse model.

2.3. COMPARISON OF THE PSD PERFORMANCE OF THE EFA AND CI ALGORITHMS

The objective of this comparison is to evaluate the neutron-gamma discrimination performance of the proposed EFA algorithm in terms of the FOM, the minimum discrimination energy, and the efficiency of neutron-gamma event separation.

The PSD performance of the EFA algorithm was evaluated by comparison with the conventional CI method. For comparison, the same set of scintillation pulses from a PuBe source, recorded according to the procedure described in the experimental section of this work, was used. For the EFA algorithm, the optimal parameter values obtained from the optimization procedure described above were used.

The integration time boundaries for the CI method were optimized by maximizing the FOM, following the approach described in [40, 41]. The optimal values of t_{start} and t_{end} were 32 ns and 142 ns, respectively, which are in good agreement with the values of 34 ns and 144 ns reported in [42]. In contrast, [19] proposed a substantially wider integration window, from 14 ns to 374 ns relative to the maximum of the scintillation pulse.

Figs. 4a, 4b presents the distributions of the PSD parameter obtained from the same set of scintillation pulses produced by the Pu–Be source using the conventional CI method and the proposed EFA algorithm.

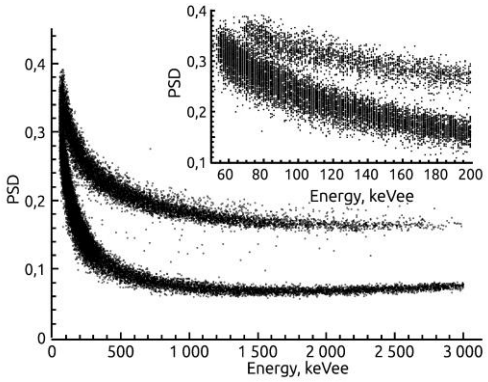


Fig. 4a. PSD distribution by the CI method

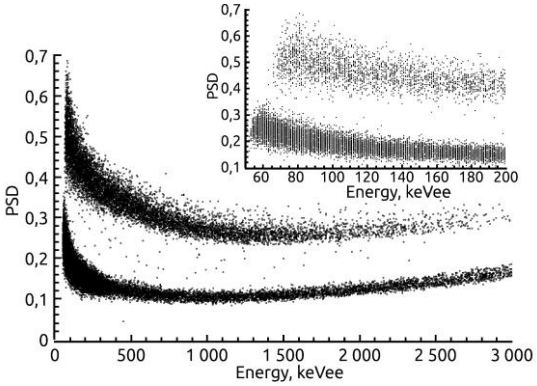


Fig. 4b. PSD distribution by the EFA algorithm

Visual comparison of the PSD parameter distributions (see Figs. 4a, 4b) shows less overlap between the neutron and gamma distributions when using the EFA algorithm, particularly in the 50…100 keVee range. Therefore, in addition to the conventional FOM, the algorithms were compared using the minimum energy at which acceptable neutron-gamma discrimination quality is still achieved. This metric complements FOM, as the latter characterizes only the degree of separation between the neutron and gamma distributions and does not fully reflect algorithm performance over the entire energy range. The relevance of this criterion is also supported by [42], which investigated PSD capabilities for low-energy neutrons at energies of approximately 80 keV.

For a qualitative comparison of the CI and EFA algorithms, Figs. 5a, 5b presents histograms of the PSD parameter distributions for the 50…100 and 100…200 keVee energy ranges, allowing their performance in the low-energy region to be assessed.

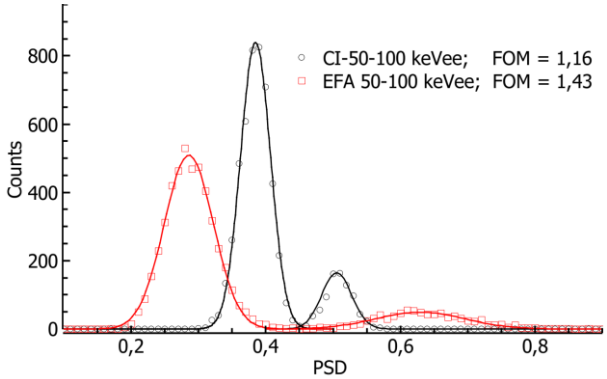


Fig. 5a. PSD distributions for CI and EFA using PuBe, 50…100 keVee

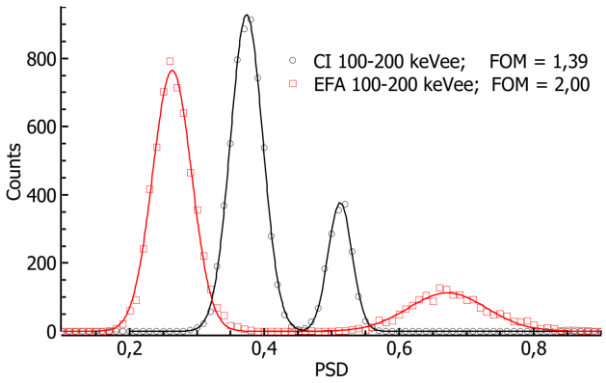


Fig. 5b. PSD distributions for CI and EFA using PuBe, 100…200 keVee

Comparison of the PSD parameter histograms (see Figs. 5a, 5b) shows better separation of neutron and gamma events when using the EFA algorithm compared with the CI method in both the 50…100 keVee and 100…200 keVee ranges. The advantage of EFA is most evident in the low-energy region, where the overlap of the distributions obtained with CI is greatest.

Quantitative comparison of the discrimination performance shows that, in the 50…100 keVee range, FOM increases from 1.16 to 1.43 (23%), while in the 100…200 keVee range it increases from 1.39 to 2.00 (44%). At the same time, the FOM achieved by EFA in the 50…100 keVee range is comparable to that achieved by CI only in the 100…200 keVee range. This indicates a reduction in the minimum energy at which reliable neutron–gamma discrimination is achieved.

To compare the performance of the CI and EFA algorithms, Fig. 6 presents the energy spectra of neutron and gamma events from the PuBe source.

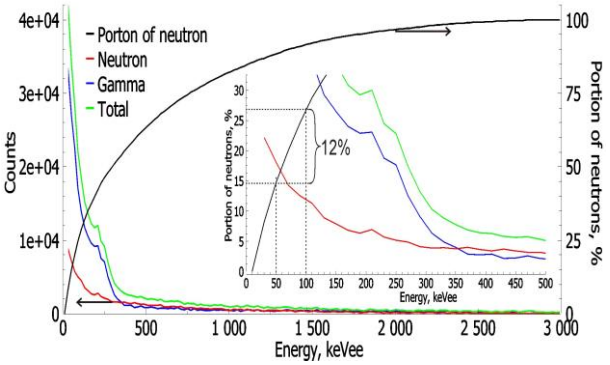


Fig. 6. Energy spectra of neutron and gamma events from the PuBe source

Analysis of the spectra shows that reducing the minimum neutron-gamma discrimination energy from 100 to 50 keVee increases the number of reliably identified neutron events by approximately 12%, which directly increases the number of reliably identified neutron and gamma events.

Thus, the proposed EFA algorithm provides better neutron-gamma discrimination than the conventional CI method without increasing computational complexity, making it promising for real-time scintillation signal processing systems.

CONCLUSIONS

A new neutron-gamma discrimination algorithm, EFA, is proposed. It is based on approximating the tail of the scintillation pulse by a sum of two exponential functions and estimating the contribution of the slow component by projecting the signal onto a physically justified basis function.

It was established that neutron and gamma events are characterized by nearly identical scintillation pulse time constants, while the main differences are determined by the ratio of the amplitudes of the slow components. This confirmed the validity of the adopted model and the use of a fixed basis function in the EFA algorithm. Optimization of the algorithm parameters showed that the highest discrimination quality is achieved for a fitting interval of 60…400 ns, while the optimal basis-function parameters are consistent with the results of fitting the averaged scintillation pulses.

Experimental comparison with the conventional CI method showed that EFA increases the FOM from 1.16 to 1.43 (23%) in the 50…100 keVee range and from 1.39 to 2.00 (44%) in the 100…200 keVee range. The discrimination quality achieved in the 50…100 keVee range is comparable to that provided by CI only in the 100…200 keVee range, indicating a reduction in the minimum energy for neutron-gamma discrimination. This increases the number of reliably identified neutron events by approximately 12%.

Thus, the proposed EFA algorithm significantly improves neutron-gamma discrimination without increasing computational complexity and is suitable for implementation in real-time digital scintillation signal processing systems. The results demonstrate the potential of physically justified scintillation pulse models for developing effective PSD algorithms suitable for real-time signal processing.

REFERENCES

1. G.F. Knoll. *Radiation Detection and Measurement* / 4th ed. Hoboken: “John Wiley & Sons”, 2010, 830 p.

2. C. Leroy, P.-G. Rancoita. *Principles of radiation interaction in matter and detection* / 4th edition. New Jersey: “World Scientific”, 2016.

3. Nondestructive Assay of Nuclear Materials for Safeguards and Security / Ed. by Geist W.H., Santi P.A., Swinhoe M.T. Cham: Springer Nature Switzerland, 2024; DOI: 10.1007/978-3-031-58277-6

4. F.D. Brooks. Development of organic scintillators // *Nuclear Instruments and Methods*. 1979, v. 162, N 1–3, p. 477-505; DOI: 10.1016/0029-554X(79)90729-8

5. J.B. Birks. *The Theory and Practice of Scintillation Counting.* London: Pergamon Press, 1967.

6. C. Grupen, B. Shwartz. *Particle Detectors* / 2nd ed. Cambridge: Cambridge University Press, 2023; DOI: 10.1017/9781009401531

7. N. Zaitseva, A. Glenn, L. Carman, et al. Pulse Shape Discrimination in Impure and Mixed Single-Crystal Organic Scintillators // *IEEE Transactions on Nuclear Science.* 2011, v. 58, N 6, p. 3411-3420; DOI: 10.1109/TNS.2011.2171363

8. Y. Kaschuck, B. Esposito. Neutron γ-ray digital pulse shape discrimination with organic scintillators // *Nucl. Instrum. Methods Phys. Res. A.* 2005, v. 551, N 2–3, p. 420-428; DOI: 10.1016/j.nima.2005.05.071

9. J.K. Polack, M. Flaska, A. Enqvist, et al. An algorithm for charge-integration, pulse-shape discrimination and estimation of neutron/photon misclassification in organic scintillators // *Nucl. Instrum. Methods Phys. Res. A.* 2015, v. 795, p. 253-267; DOI: 10.1016/j.nima.2015.05.048

10. H. Liu, Y. Zhan, M. Liu, et al. Pulse shape discrimination algorithms: Survey and benchmark // *Radiation Measurements*. 2026, v. 193, p. 107653; DOI: 10.1016/j.radmeas.2026.107653

11. Z.W. Bell. Tests on a digital neutron-gamma pulse shape discriminator with NE213 *// Nucl. Instrum. Methods Phys. Res.* 1981, v. 188, N 1, p. 105-109; DOI: 10.1016/0029-554X(81)90327-X

12. A.D. Kaplan, B. Blair, C. Chen, et al. A neutron-gamma pulse shape discrimination method based on pure and mixed sources // *Nucl. Instrum. Methods Phys. Res. A.* 2019, v. 919, p. 36-41; DOI: 10.1016/j.nima.2018.11.136

13. N. Zaitseva, A. Glenn, L. Carman, et al. Scintillation properties of solution-grown trans-stilbene single crystals // *Nucl. Instrum. Methods Phys. Res. A*. 2015, v. 789, p. 8-15; DOI: 10.1016/j.nima.2015.03.090

14. J. Zhou, A. Abdulaziz, Y. Altmann, A.D. Fulvio. Generalized Method for the Optimization of Pulse Shape Discrimination Parameters // *Nucl. Instrum. Methods Phys. Res. A.* 2023, v. 1050, p. 168184; DOI: 10.1016/j.nima.2023.168184

15. C. Liao, H. Yang. Pulse shape discrimination using EJ-299-33 plastic scintillator coupled with a Silicon Photomultiplier array // *Nucl. Instrum. Methods Phys. Res. A.* 2015, v. 789, p. 150-157; DOI: 10.1016/j.nima.2015.04.016

16. G. Ranucci. A review of the statistical foundations of the classical pulse shape discrimination techniques in scintillation applications // *IEEE Nucl. Sci. Symp. Conf. Rec.* Rome, Italy: IEEE, 2004, v. 2, p. 804-809; DOI: 10.1109/NSSMIC.2004.1462331

17. K.A.A. Gamage, M.J. Joyce, N.P. Hawkes. A comparison of four different digital algorithms for pulse-shape discrimination in fast scintillators // *Nucl. Instrum. Methods Phys. Res. A.* 2011, v. 642, N 1, p. 78-83; DOI: 10.1016/j.nima.2011.03.065

18. L. Adamowski, M. Grodzicka-Kobylka, T. Szczesniak, et al. Influence of Self-Absorption on Pulse Shape Discrimination in Organic Glass Scintillators. arXiv, 2025; DOI: 10.48550/arXiv.2505.08513

19. N. Gaughan, J. Zhou, F.D. Becchetti, et al. Characterization of stilbene-d12 for neutron spectroscopy without time of flight // *Nucl. Instrum. Methods Phys. Res. A.* 2021, v. 1018, p. 165822;

DOI: 10.1016/j.nima.2021.165822

20. M. Sénoville, F. Delaunay, M. Pârlog, et al. Neutron- γ discrimination with organic scintillators: Intrinsic pulse shape and light yield contributions // *Nucl. Instrum. Methods Phys. Res. A.* 2020, v. 971, p. 164080; DOI: 10.1016/j.nima.2020.164080

21. A.C. Kaplan, M. Flaska, A. Enqvist, et al. EJ-309 pulse shape discrimination performance with a high gamma-ray-to-neutron ratio and low threshold // *Nucl. Instrum. Methods Phys. Res. A.* 2013, v. 729, p. 463-468; DOI: 10.1016/j.nima.2013.07.081

22. A.D. Kaplan, B. Blair, A. Glenn, R. Wurtz. Automated integration gate selection for Gaussian mixture model pulse shape discrimination // *Nucl. Instrum. Methods Phys. Res. A.* 2023, v. 1055, p. 168486; DOI: 10.1016/j.nima.2023.168486

23. Y. Lee, J. Kim, B. Koh, et al. Pulse shape discrimination in an organic scintillation phoswich detector using machine learning techniques // *Frontiers in Physics*. 2024, v. 12, p. 1361608;
DOI: 10.3389/fphy.2024.1361608

24. Hamamatsu. "New_Hamamatsu – Catalog Hamamatsu-PMT-New".

25. G. Van Rossum, F.L. Drake Jr. *The Python Language Reference*. Release 2.6.4. Python Software Foundation, 2010.

26. W.R. Leo. *Techniques for Nuclear and Particle Physics Experiments: A How-to Approach.* Berlin, Heidelberg: Springer Berlin Heidelberg, 1994; DOI: 10.1007/978-3-642-57920-2

27. Hamamatsu. *Photomultiplier Tubes: Basics and Applications* / 4th ed. Hamamatsu Photonics K.K., 2007.

28. J. Iwanowska-Hanke, M. Moszynski, L. Swiderski, et al. Comparative study of large samples (2"×2") plastic scintillators and EJ309 liquid with pulse shape discrimination (PSD) capabilities // *Journal of Instrumentation.* 2014, v. 9, N 06, p. 06014;
DOI: 10.1088/1748-0221/9/06/P06014

29. D.L. Horrocks. Pulse Shape Discrimination with Organic Liquid Scintillator Solutions // *Applied Spectroscopy*. 1970, v. 24, p. 397-404;
DOI:10.1366/000370270774371435

30. F.T. Kuchnir, F.J. Lynch. Time Dependence of Scintillations and the Effect on Pulse-Shape Discrimination // *IEEE Transactions on Nuclear Science.* 1968, v. 15, N 3, p. 107-113;
DOI: 10.1109/TNS.1968.4324923

31. W. Becker. *Advanced Time-Correlated Single Photon Counting Techniques* / 1st ed. with Castleman A.W., Toennies J.P. Berlin, Heidelberg: Springer Berlin / Heidelberg, 2005, 404 p. (Springer Series in Chemical Physics Ser.).

32. L.M. Bollinger, G.E. Thomas. Measurement of the Time Dependence of Scintillation Intensity by a Delayed-Coincidence Method // *Review of Scientific Instruments*. 1961, v. 32, N 9, p. 1044-1050;
DOI: 10.1063/1.1717610

33. P. Harihar, H. Chen, W.J. Stapor, A.R. Knudson. Scintillation decays in a trans-stilbene crystal // *Nucl. Instrum. Methods Phys. Res. A.* 1993, v. 336, N 1–2, p. 76-178; DOI: 10.1016/0168-9002(93)91094-4

34. M. Murugesan, R. Paulraj, M. Tyagi, et al. <100> directed growth, Hirshfeld surface analysis, and scintillation properties of trans-Stilbene (TSB) single crystal grown by modified low-temperature vertical Bridgman method // *Journal of Materials Science: Materials in Electronics.* 2021, v. 32, N 11, p. 15200-15210; DOI: 10.1007/s10854-021-06072-5

35. H.D. Kim, G.S. Cho, H.J. Kim. Characteristics of a stilbene scintillation crystal in a neutron spectrometer // *Radiation Measurements*. 2013, v. 58, p. 133-137; DOI: 10.1016/j.radmeas.2013.01.004

36. N.Z. Galunov, I.F. Khromiuk, O.A. Tarasenko. Features of pulse shape discrimination capability of organic heterogeneous scintillators // *Nucl. Instrum. Methods Phys. Res. A.* 2020, v. 949, p. 162870;
DOI: 10.1016/j.nima.2019.162870

37. G.T. Wright. Scintillation Decay Times of Organic Crystals // *Proceedings of the Physical Society. Section B.* 1956, v. 69, N 3, p. 358-372;
DOI: 10.1088/0370-1301/69/3/311

38. G. Laustriat. The luminescence decay of organic scintillators // *Molecular Crystals*. 1968, v. 4, N 1-4, p. 127-145; DOI: 10.1080/15421406808082905

39. M. Grodzicka-Kobylka, T. Szczesniak, M. Moszyński, et al. 2 inch molecular organic glass scintillator for neutron-gamma discrimination // *Nucl. Instrum. Methods Phys. Res. A.* 2023, v. 1047, p. 167702;
DOI: 10.1016/j.nima.2022.167702

40. I.A. Pawełczak, S.A. Ouedraogo, A.M. Glenn, et al. Studies of neutron-γ pulse shape discrimination in EJ-309 liquid scintillator using charge integration method // *Nucl. Instrum. Methods Phys. Res. A.* 2013, v. 711, p. 21-26; DOI: 10.1016/j.nima.2013.01.028

41. Z. Wang, J. Zeng, T. Zhu, et al. Optimization of integration limit in the charge comparison method based on signal shape function // *Nucl. Instrum. Methods Phys. Res. A.* 2014, v. 760, p. 5-9;
DOI: 10.1016/j.nima.2014.05.017

42. A. Di Chicco, M. Petit, R. Jacqmin, et al. Investigation of the neutron-gamma ray discrimination performance at low neutron energy of a solution-grown stilbene scintillator // *EPJ Web of Conferences*. 2020, v. 225, p. 04013; DOI: 10.1051/epjconf/202022504013

Article received 08.09.2026

АПРОКСИМАЦІЙНИЙ АЛГОРИТМ ДЛЯ НЕЙТРОН-ГАММА-РОЗДІЛЕННЯ

В.О. Новгородцев, О.В. Колесніков

Запропоновано новий алгоритм нейтрон-гамма-розділення Exponential Function Approximation (EFA) для органічних сцинтиляційних детекторів. Алгоритм ґрунтується на апроксимації хвостової частини сцинтиляційного імпульсу базисною функцією, що являє собою суму двох експоненціальних компонент із фіксованими сталими часу. Оптимізацію параметрів алгоритму виконано за критерієм максимуму параметра якості нейтрон-гамма-розділення (FOM). Експериментальна перевірка на сцинтиляційних імпульсах від джерела PuBe показала, що запропонований алгоритм забезпечує підвищення FOM із 1,16 до 1,43 (на 23%) у діапазоні енергій 50…100 кеВее та з 1,39 до 2,00 (на 44%) у діапазоні 100…200 кеВее, як порівняти з класичним методом інтегрування заряду (CI). Досягнута алгоритмом EFA якість розділення в діапазоні 50…100 кеВее є порівнянною з якістю, яку метод CI забезпечує лише в діапазоні 100…200 кеВее, що свідчить про зниження мінімальної енергії нейтрон-гамма-розділення та забезпечує збільшення кількості надійно ідентифікованих нейтронних подій приблизно на 12%. Показано, що алгоритм EFA є узагальненням методу CI і в граничному випадку, коли базисна функція тотожно дорівнює одиниці, зводиться до нього. Запропоновано варіант реалізації EFA з обчислювальною складністю, близькою до методу CI.